Sensors & Actuators: B. Chemical 461 (2026) 139957

Contents lists available at ScienceDirect

Sensors and Actuators: B. Chemical

journal homepage: www.elsevier.com/locate/snb

3D DNA walker-powered biological field-effect-transistors (BioFETs) for ultrasensitive cancer exosome detection

Quan Wang [a], Xiao Shu [a], Wen Yin [a], Haitian Chen [d], Xijing Yan [c], Keyu Yao [a], Duo Wai-Chi Wong [a], Mo Yang [a,e,f,*], Kunpeng Hu [c,**], Jingyu Shi [a,**], James Chung-Wai Cheung [a,b,*]

[a] Department of Biomedical Engineering, The Hong Kong Polytechnic University, Kowloon, Hong Kong 999077, China
[b] Research Institute for Smart Ageing, The Hong Kong Polytechnic University, Kowloon, Hong Kong 999077, China
[c] Department of Breast and Thyroid Surgery, Lingnan Hospital, The Third Affiliated Hospital of Sun Yat-sen University, Guangzhou 510630, China
[d] Department of Hepatic Surgery and Liver Transplantation Center of The Third Affiliated Hospital of Sun Yat-sen University, Guangzhou 510630, China
[e] The Hong Kong Polytechnic University Shenzhen Research Institute, Shenzhen 518000, China
[f] Joint Research Center of Biosensing and Precision Theranostics, The Hong Kong Polytechnic University, Kowloon, Hong Kong 999077, China

ARTICLE INFO

Keywords:
DNA walker
BioFETs
Exosomes
HER2 breast cancer
Detection

ABSTRACT

Exosomes (30–150 nm) are phospholipid nanovesicles that carry molecular cargo reflecting their cellular origin, making them promising non-invasive biomarkers for cancer detection. Herein, we report the first 3D DNA walker-powered graphene field-effect transistor (GFET) biosensing platform for ultrasensitive detection of HER2-positive breast cancer exosomes. The assay integrates a two-stage, cascade amplification strategy. First, specific recognition of HER2-positive exosomes induces aptamer displacement, thereby activating DNAzyme-powered 3D DNA walkers that catalytically cleave substrate strands in the presence of Zn^{2+}, continuously releasing single-stranded DNA (ssDNA) reporters. Second, the released ssDNA is captured by hairpin probes at the GFET gate interface, increasing the local negative charge within the Debye screening length and producing a shift in the charge neutrality point voltage (V_{cnp}). By measuring the signal change, the platform enables quantitative detection within ~1.5 h and achieves a limit of detection (LOD) of 1.57 particles μL^{-1}. Furthermore, this DNA walker-powered GFET platform was validated using clinical plasma samples and successfully distinguished HER2-positive from HER2-negative breast cancer patients.

1. Introduction

Exosomes are nanoscale extracellular vesicles found in body fluids, rich in nucleic acids and proteins reflecting their origin cells. Due to their stability and abundance, exosomes have become promising non-invasive biomarkers for cancer detection [1]. In breast cancer, human epidermal growth factor receptor 2 (HER2) is an important clinical biomarker used to define molecular subtypes and to guide targeted therapy [2]. Therefore, HER2 enrichment on tumor-derived exosomes offers the possibility of assessing HER2 status via liquid biopsy [3]. However, traditional exosome analysis methods, such as Western blotting (WB) and enzyme-linked immunosorbent assay (ELISA), are labor-intensive, time-consuming, and often have limited sensitivity, thus restricting their clinical application [4–6]. To overcome these limitations, a variety of biosensing strategies have been developed for cancer exosome detection, including electrochemical [7,8], fluorescence-based [9,10], and surface-enhanced Raman scattering (SERS)-based [11] biosensors. Among these methods, biological field-effect transistors (BioFETs) are particularly attractive because they directly convert biomolecular binding events on the sensor surface into electrical signals by modulating the local electrostatic potential of the semiconductor channel [12,13]. For example, label-free exosome detection has been demonstrated using CD63 antibody-functionalized silicon nanowire FETs [14] and graphene FETs [15]. In particular, graphene FETs are attractive for liquid-biopsy analysis because graphene is highly sensitive to interfacial charge changes and enables direct electrical readout of

* Corresponding authors at: Department of Biomedical Engineering, The Hong Kong Polytechnic University, Kowloon, Hong Kong 999077, China.
** Corresponding authors.
E-mail addresses: yang@polyu.edu.hk (M. Yang), hukpeng@mail.sysu.edu.cn (K. Hu), jing-yu.shi@polyu.edu.hk (J. Shi), james.chungwai.cheung@polyu.edu.hk (J.C.-W. Cheung).

https://doi.org/10.1016/j.snb.2026.139957
Received 2 February 2026; Received in revised form 31 March 2026; Accepted 8 April 2026
Available online 14 April 2026

biomolecular recognition events [16,17]. However, many reported FET-based exosome sensors require highly diluted systems to increase the Debye screening length, thereby deviating from physiological ionic conditions and compromising practical sensitivity. This challenge stems from the Debye screening effect in physiological solutions, where the short Debye length (< 0.7 nm) severely attenuates electrical signals from targets located away from the sensor surface [18]. Additionally, nonspecific adsorption and limited intrinsic signal amplification severely restrict sensitivity for low-abundance targets [19]. Therefore, effective signal-amplification strategies are essential to enhance FET performance for clinically relevant exosome detection.

DNA walkers are autonomous nucleic acid nanomachines capable of cyclic signal amplification. By continuously walking along nucleic acid orbitals, a single target recognition event can be translated into the generation of multiple nucleic acid outputs, thereby boosting detectable signal levels [20]. Compared with PCR-based or enzyme-dependent approaches that require thermal cycling or complex reagent handling, DNA walkers provide programmable operation under mild conditions, improving analytical sensitivity while maintaining operational simplicity [21–23]. Notably, DNA walker systems that release multiple short, highly charged ssDNA products are particularly attractive for FET sensing, because these reporters can be captured directly on the transistor surface to (i) increase the number of charge-modulation events and (ii) position the charge close to the sensing interface, thereby alleviating Debye screening. These features make DNA walker-based amplification highly suitable for integration with bioelectronic biosensing formats for liquid biopsy applications [24]. To date, DNA walker-based biosensors have been mainly integrated with electrochemical, fluorescence, or colorimetric readouts [25–28]. However, to the best of our knowledge, integrating DNA walker-driven signal amplification with FET-based electrical signal conversion has not been reported.

Herein, we developed a graphene field-effect transistor (GFET) biosensing platform integrating 3D DNA walkers for ultrasensitive detection of exosomes derived from HER2-positive breast cancer cells. In this system, gold nanoparticles (AuNPs) functionalized with substrate strands served as high-density 3D walking tracks. A Zn^{2+} specific DNAzyme, acting as the walking strands, was initially hybridized and locked by a HER2-specific aptamer, and subsequently immobilized onto the AuNPs surface. Upon recognition of HER2-positive exosomes, aptamer binding triggers the unlocking of DNAzyme walking strands, initiating a Zn^{2+}-driven cyclic walking process that cleaves substrate strands at the rA site and releases numerous short ssDNA fragments. These ssDNA products are subsequently captured by complementary hairpin (Hp) probes immobilized on the GFET surface, positioning the charged hybrids near the sensing interface to generate a measurable electrical response. By monitoring shifts in the charge neutrality point (V_{cnp}), the DNA walker-powered GFET platform achieved rapid, label-free, and ultrasensitive detection of exosomes with a limit of 1.57 particles μL^{-1}, and successfully distinguished HER2-positive from HER2-negative exosomes in clinical plasma samples.

2. Materials and methods

The full experimental procedure, chemicals, and instrumentation used in the study were provided in the Supporting Information.

3. Results and discussion

3.1. Working principle of 3D DNA walker-powered BioFETs for cancer exosomes detection

The working principle of the 3D DNA walker-powered GFET platform is illustrated in Scheme 1. In this design, AuNPs serve as 3D scaffolds and are co-functionalized with substrate strands and Zn^{2+}-dependent DNAzyme walking strands [29] at an optimized ratio. Each DNAzyme walking strand is partially hybridized at its 3′ terminus with a HER2-specific aptamer [3,30,31], which serves as a locking element to keep the walker inactive while providing target specificity. Upon exposure to HER2-positive exosomes, the aptamer binds to HER2

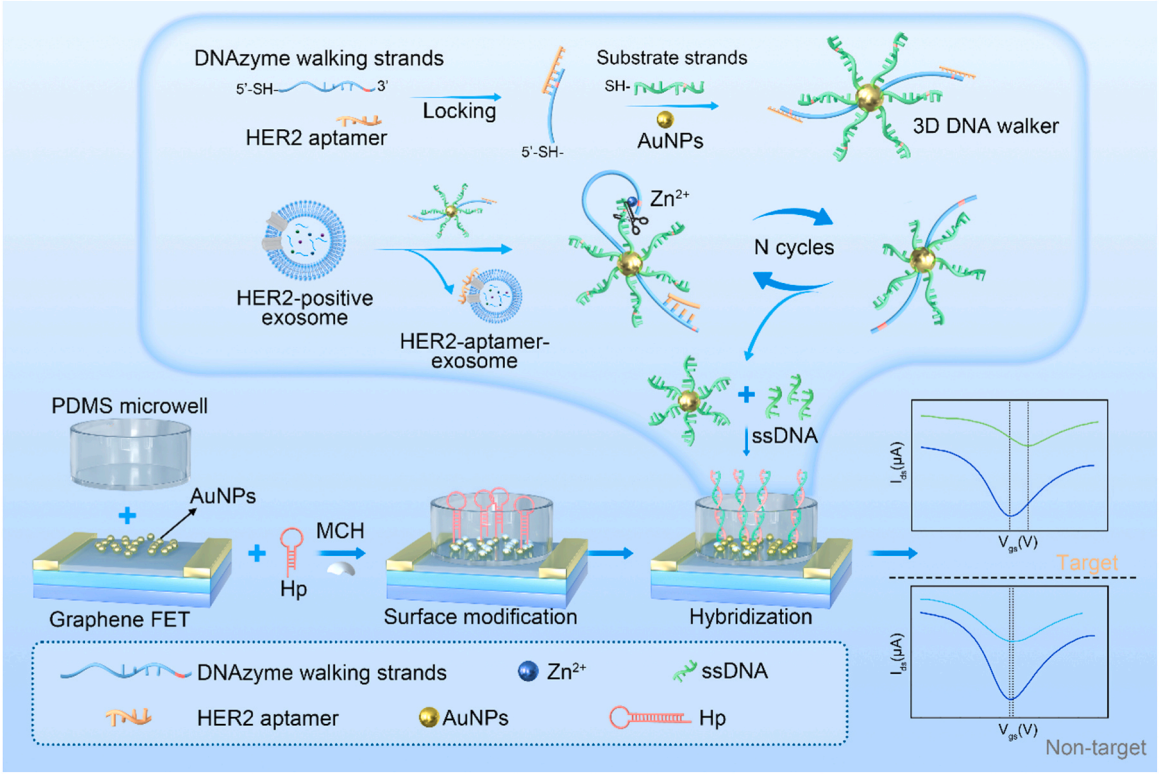

Scheme 1. Working principle of 3D DNA walker-powered BioFETs for ultrasensitive cancer exosomes detection.

proteins on the exosome surface and dissociates from the walking strand, thereby activating the DNAzyme. In the presence of Zn^{2+}, the activated walker cyclically cleaves the substrate strands anchored on the AuNP surface, producing abundant ssDNA fragments. This constitutes the first amplification step, converting a single exosome-recognition event into multiple ssDNA outputs.

The ssDNA products are subsequently introduced to the GFET gate region, where complementary Hp probes are thermally annealed into a stable hairpin structure and immobilized on the AuNP-GFET surface through Au−S bonds. A micro-PDMS well was positioned over the GFET gate region as a confined reaction chamber to avoid electrode contamination and suppress environmental noise. The released ssDNA hybridizes with the Hp probes and opens the hairpin structure, bringing additional negative charges into close proximity to the graphene surface. This process changes the local electrostatic environment on the graphene channel within the Debye shield length and shifts the GFET transfer curve. The electrical response is quantified by the corresponding shift in V_{cnp}, where V_{cnp} denotes the charge neutrality point of graphene. In this way, the GFET acts as an inherent signal amplifier by converting subtle interfacial charge changes into a measurable electrical response. In contrast, in the absence of HER2-positive exosomes, the DNA walker remains locked, substrate cleavage is suppressed, and the hairpin probes remain closed, resulting in only a weak electrical response. Therefore, this cascade design enables rapid, highly specific, and ultrasensitive detection of HER2-positive exosomes.

3.2. *Exosomes characterization and feasibility verification of 3D DNA walkers*

As shown in Fig. 1a, transmission electron microscopy (TEM) revealed that SKBR3 exosomes have a characteristic bowl-shaped morphology with an average diameter of 100 nm. Nanoparticle

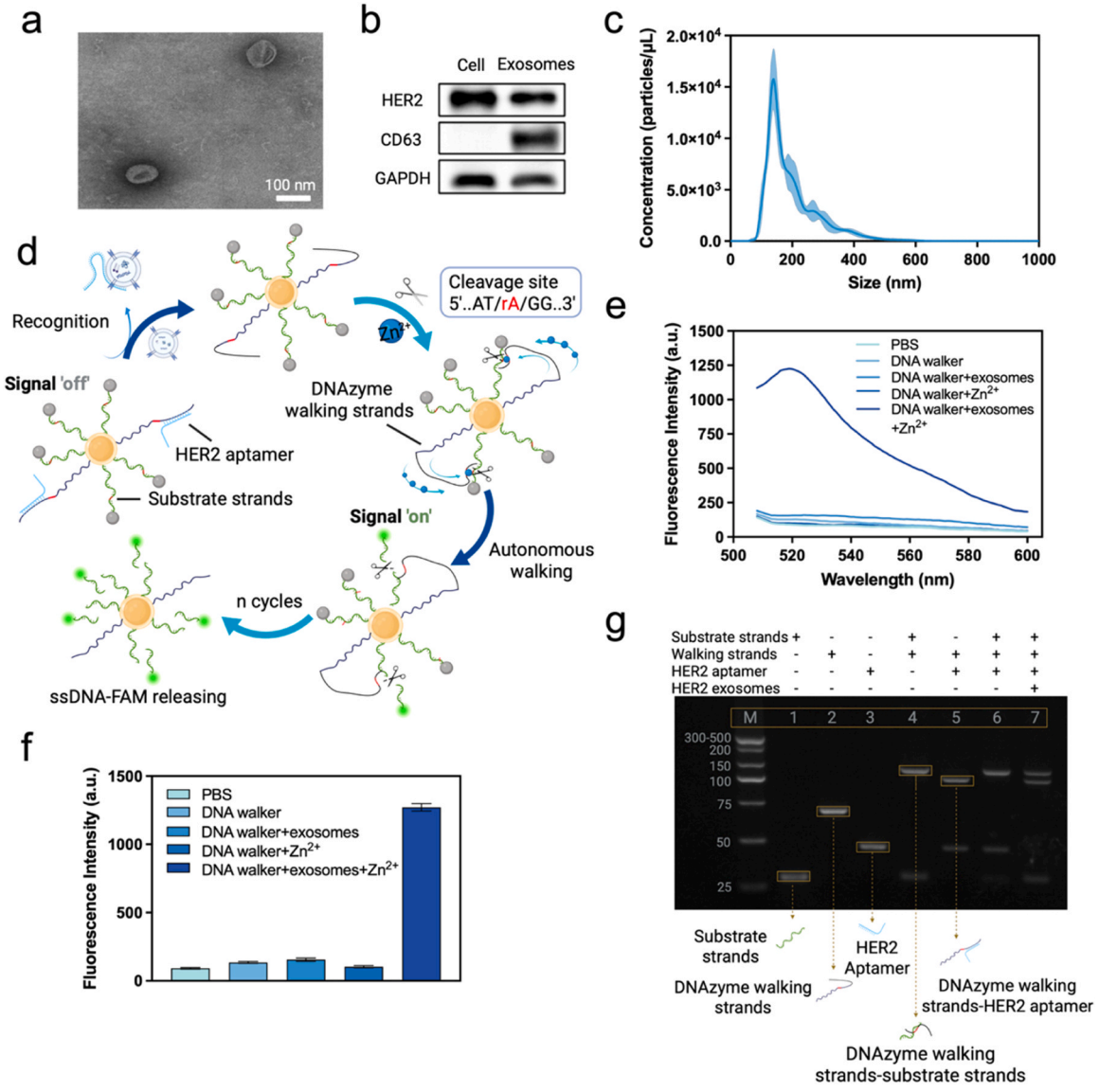

Fig. 1. Exosome characterization and feasibility verification of DNA walkers. (a) TEM image of isolated exosomes derived from SKBR3 cell lines. (b) Western blot analysis of HER2, CD63, and GAPDH in SKBR3 cells and their isolated exosomes. (c) Size distribution of exosomes obtained by NTA. (d) Schematic illustration of the target-triggered autonomous DNA walkers process with fluorescent readout. (e) Fluorescence spectra of the DNA walkers obtained in the presence of different reagents. $C_{exosomes} = 10^4$ particles/μL, incubation conditions: 3 h, 37 °C. (f) Corresponding quantitative analysis of fluorescence intensity across different reaction conditions. (g) PAGE images of DNA ladder, (1) substrate strands, (2) DNAzyme walking strands, (3) HER2 aptamer, (4) DNAzyme walking strands/substrate strands, (5) DNAzyme walking strands/HER2 aptamer, (6) DNAzyme walking strands/HER2 aptamer/substrate strands, (7) DNAzyme walking strands/HER2 aptamer/substrate strands/HER2-positive exosomes.

tracking analysis (NTA) revealed a unimodal size distribution with a mean particle diameter of 139 nm (Fig. 1c). The slightly larger size than TEM was expected because NTA measured the hydrodynamic diameter in solution. Western blot analysis confirmed the exosomal protein profile (Fig. 1b). CD63 was enriched in the isolated vesicles, indicating successful exosome isolation. HER2 was highly expressed in both SKBR3 cells and the derived exosomes, suggesting that the released exosomes retained the HER2 membrane protein characteristics of the parental cancer cells [32].

To verify the feasibility of the 3D DNA walker, we performed a fluorescence assay (Fig. 1d). FAM-labeled substrate strands and aptamer-locked DNAzyme walking strands were co-immobilized on AuNPs, resulting in an initial "off" signal due to Au-induced fluorescence quenching. Upon addition of target exosomes, the high-affinity binding interaction between the HER2 aptamer and HER2 exosomes unlocked the DNAzyme walking strands. In the presence of Zn^{2+}, the activated walker cleaved the substrate at the rA site and released FAM-labeled ssDNA fragments, restoring fluorescence ("on"). This cyclic walking-and-cleavage process continuously generated fluorescent signals, thereby amplifying the signal. As shown in Fig. 1e, a strong fluorescence increase at 520 nm was observed only when both HER2-positive exosomes and Zn^{2+} were present, whereas all control groups showed negligible signals. The corresponding quantitative fluorescence analysis further confirmed this observation (Fig. 1f). To confirm the DNA walking mechanism, polyacrylamide gel electrophoresis (PAGE) was performed (Fig. 1g). Substrate strands, DNAzyme walking strands, and HER2 aptamer appeared as distinct single bands in lanes 1, 2, and 3, respectively. Additional bands corresponding to the DNAzyme walking strands–substrate strands complex and the DNAzyme walking strands–HER2 aptamer complex were observed in lanes 4 and 5, respectively. In the presence of target exosomes (lane 7), the DNAzyme walking strands–substrate strands band was evident, consistent with exosome-triggered aptamer dissociation and subsequent binding of the released DNAzyme walking strand to the substrate strand.

We optimized the operating conditions of the 3D DNA walker. First, we screened the DNAzyme-to-substrate molar ratio and observed the highest fluorescence enhancement ($F_1/F_0 < 18$) at 1:17 (Fig. S1a). This optimized ratio was therefore used for subsequent AuNP conjugation. To estimate the strand loading, substrate coverage per AuNP was quantified by a fluorescence displacement assay using FAM-labeled substrate strands as tracers. Briefly, the AuNP-DNA conjugates were incubated overnight with 2-ME in Tris-HCl buffer to displace the surface-bound thiolated DNA, and the released FAM strands in the supernatant were quantified using a calibration curve (Fig. S2). The average number of substrate strands was ~127 per AuNP, which corresponds to ~7 DNAzyme walking strands per AuNP based on the optimized 17:1 substrate: DNAzyme feeding ratio. Second, kinetic studies (10–180 min) showed the signal reached ~80% of maximum by 60 min and plateaued by 90 min, so 60 min was selected as the optimal reaction time (Fig. S1b). The DNA walker exhibited the best activity at 37 °C and pH 7.4 (Fig. S1c-d). To evaluate robustness against nonspecific protein effects, we tested the assay in the presence of BSA (1 mg/mL). The fluorescence response remained > 95% of the protein-free control (Fig. S1e). Finally, the effects of different metal ions on DNA walker activity were investigated, and Zn^{2+} was selected as the cofactor for the 8–17E DNAzyme because it produced the highest fluorescence intensity among the tested ions, along with its good biocompatibility and tight physiological regulation [33]. The inset further shows that the fluorescence intensity reached a maximum at 1.0 mM Zn^{2+} (Fig. S1f). Because endogenous Zn^{2+} levels in serum are much lower, Zn^{2+} is supplemented as an assay reagent. We further performed Dynamic Light Scattering (DLS) to evaluate exosome stability in the presence of Zn^{2+} at different incubation times (5–60 min) (Fig. S3). The hydrodynamic diameter showed negligible change across the tested times, indicating no apparent Zn^{2+}-induced vesicle aggregation or gross membrane disruption within 60 min. Although a moderate increase in PDI was observed, this did not result in a measurable decrease in the detection readings during the sensing response time. Therefore, the optimal operating conditions for the 3D DNA walker were determined to be a DNAzyme-to-substrate feeding ratio of 1:17, a reaction time of 60 min, and an incubation environment of 37 °C at pH 7.4 with 1.0 mM Zn^{2+} as the cofactor, which were used for all subsequent experiments.

3.3. Establishment and functionalization of the GFETs platform

AuNPs-GFETs were used as a substrate to immobilize Hp probes to capture ssDNA fragments released after the 3D DNA walking reaction (Fig. 2a). Initially, thiolated-Hp probes were covalently linked to the AuNP surface through Au-S bonds, and MCH was used as a filler to improve probe orientation and reduce nonspecific adsorption. Subsequently, ssDNA fragments released from the DNA walker were incubated with the Hp-functionalized AuNPs-GFET for 30 min, triggering the opening and hybridization of the hairpin structure, thereby altering the local charge distribution near the graphene channel and generating measurable Dirac point shifts for exosome quantitative analysis. Device morphology was characterized by SEM, which showed well-defined source-drain electrodes and a continuous sensing channel (Fig. 2b). EDS elemental analysis detected Si, O, C, and Au, consistent with the Si/SiO_2 substrate, graphene channel, and AuNP decoration (Fig. S4-5). DNA modification and target hybridization were further verified by XPS. After Hp probes immobilization, characteristic peaks emerged at 162.25 eV (S_{2p}), 133.41 eV (P_{2p}), and 400.08 eV (N_{1s}), confirming successful DNA attachment on AuNPs and the presence of the DNA backbone and nucleobases (Fig. 2e-g). Upon hybridization with the complementary ssDNA, increased P_{2p} and N_{1s} intensities indicate additional nucleic acid bound on the surface (Fig. 2f-g). Atomic force microscopy (AFM) analysis showed increased surface roughness after Hp functionalization (Rq from 1.144 nm to 2.209 nm, Ra from 0.814 nm to 1.478 nm, and Rz from 13.875 nm to 38.399 nm), indicating the successful Hp modification (Fig. 2c-d). The pristine GFET surface before modification is shown in Fig. S6. To assess surface uniformity, Kelvin probe force microscopy (KPFM) was used to map the surface potential of AuNPs-GFET after Hp modification. The KPFM images displayed a spatially uniform potential distribution, indicating uniform Hp coverage (Fig. S7a). The average KPFM surface potential decreased from 134.847 to 52.394 mV, consistent with the introduction of negatively charged DNA probes, while reduced lateral potential dispersion (Sq: 12.592–3.289 mV; calculated CV: 9.29–6.27%) suggests a more homogeneous Hp distribution across the AuNPs–GFET surface (Fig. S7b).

3.4. The reliability of 3D DNA walker-powered GFET platform

The charge-neutrality point voltage (V_{cnp}), also known as the Dirac point voltage, was determined from the transfer characteristics of graphene FETs to evaluate device performance. V_{cnp} was identified as the gate voltage corresponding to the minimum drain current in the I_{ds}-V_{gs} transfer curve, where the electron and hole carrier concentrations are equal at the graphene channel. The reproducibility of GFETs was assessed by measuring transfer curves of eight sensing channels at a constant drain-source bias of 50 mV (Fig. 3a). All channels exhibited nearly superimposable I_{ds}–V_{gs} curves with V_{cnp} converging around 180 mV. Device stability was then confirmed by monitoring transfer curves of a single GFET over 120 min with PBS buffer (Fig. 3b). The V_{cnp} remained stable ($\Delta V_{cnp} < 2$ mV) with on- and off-state currents varying by less than 3%, indicating stable graphene channel and electrode interfaces in the assay buffer. Quantitative analysis further showed that V_{cnp} for all eight channels clustered tightly between 176.5 and 180.5 mV (mean = 178.5 mV, $\sigma = 1.2$ mV, variability < 1%), confirming the homogeneous doping state of the graphene channel across all devices (Fig. 3c). After the Hp modification, the V_{cnp} maintained within a narrow range between 345 and 360 mV with a RSD of 1.47% across all sensing channels, when the devices were stored at 4°C in a humid

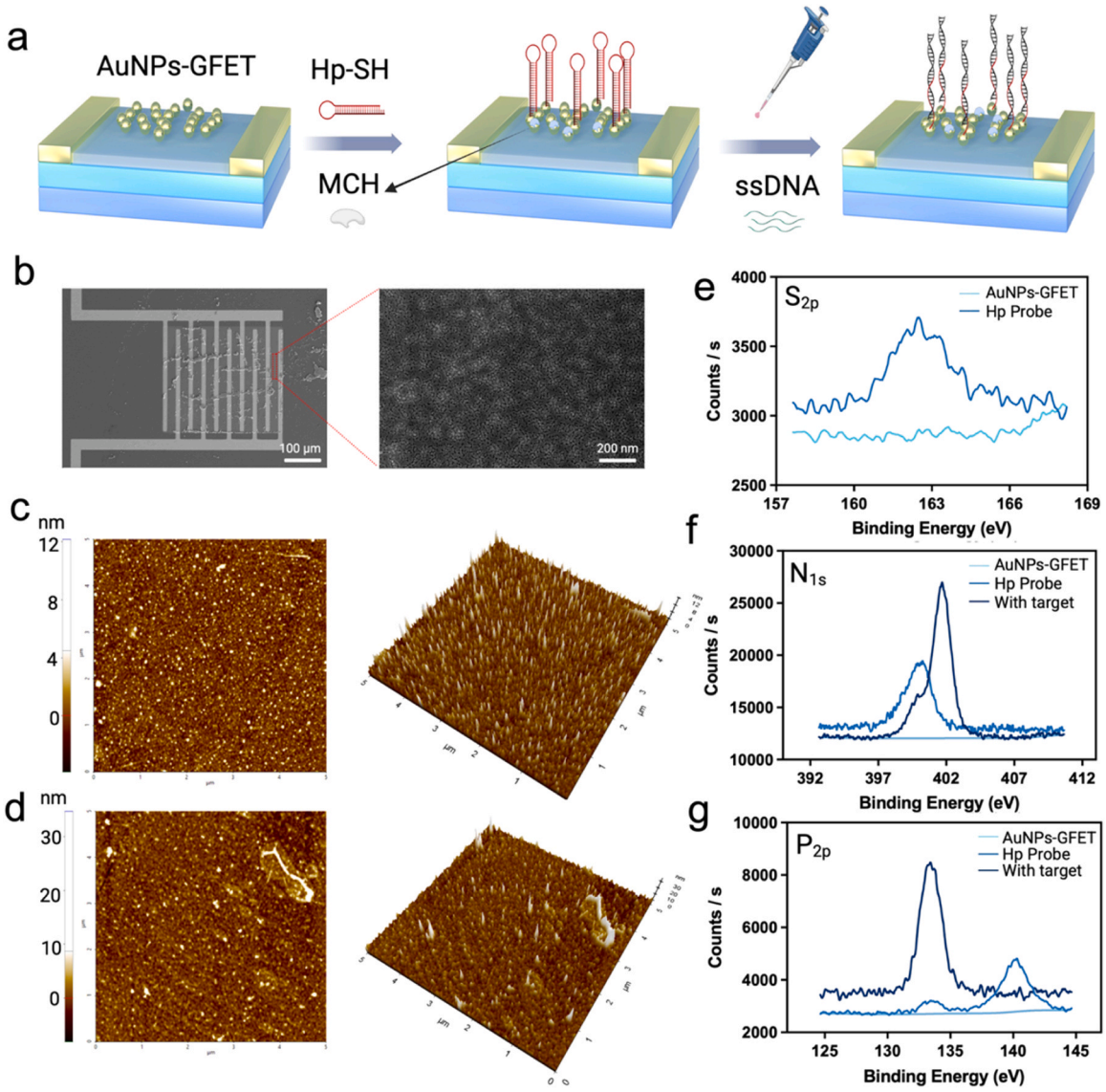

Fig. 2. Establishment and functionalization of GFETs. (a) Schematic illustration of Hp and MCH modification on AuNPs-GFET. (b) SEM images of AuNPs-GFET sensing channel structure and the graphene layer surface. 2D and 3D AFM profile of the GFET surface after AuNPs decoration (c) and Hp functionalization (d). (e-g) XPS analysis of AuNPs-GFET surface: S_{2p} (e), N_{1s} (f), and P_{2p} (g) peaks at different modification stages (before/after Hp functionalization and during detection).

environment between measurements. These narrow distributions indicate that subsequent biosensing shifts arise from target-induced charge transfer rather than inherent device fluctuations. The stability of GFETs after Hp modification was further verified by measuring the transfer characteristics at multiple time intervals, showing that V_{cnp} remained stable over 7 h (Fig. 3d-e). These results confirm that the Hp-modified GFET maintains negligible electrical drift during the probe immobilization phase, validating its suitability for subsequent DNA walker-mediated amplification and subsequent detection.

To confirm detection capability, we recorded the transfer characteristics at three sequential stages: (i) baseline (AuNPs-GFET), V_{cnp} = 178.5 mV, (ii) after immobilization of Hp onto AuNP-GFET surface (Hp-AuNP-GFET), V_{cnp} = 350 mV, and (iii) after exposure to the DNA-walker reaction products (ssDNA) generated in the presence of 10^4 particles/μL HER2-positive exosomes, V_{cnp} = 445 mV (Fig. 3f). The positive shift from 178.5 mV to 350 mV after Hp immobilization is attributed to the formation of a negatively charged DNA layer near graphene. The Hp probes immobilized on AuNPs through Au-S bonds present a constrained double-helix stem structure with partially confined phosphate backbone, resulting in an initial p-doping effect with a modest V_{cnp} rightward shift. The further shift from 350 mV to 445 mV after sample addition arises from the accumulation of DNA walker-generated ssDNA reporters on the surface via hybridization with Hp. These ssDNA present all phosphate groups in an extended conformation that maximizes exposure to the graphene electrostatic environment, producing a substantially stronger p-doping effect. The further shift is attributed to accumulated negatively charged ssDNA, which dominates the overall signal via DNA walker amplification, thereby explaining the robust signal amplification. This ssDNA-induced signal (ΔV_{cnp} = 95 mV) dramatically exceeded the minimal baseline noise (< 2 mV), demonstrating high signal-to-noise detection.

3.5. *The performance of 3D DNA walker-powered GFET platform for HER2-positive exosomes detection*

The DNA walker-powered GFET platform enabled the quantitative detection of exosomes across a wide concentration range (0.1–10^4 particles/μL), as evidenced by a monotonic increase in V_{cnp} shift with HER2-positive exosomes concentrations, as shown in Fig. 4a. This concentration-dependent behavior reflects the direct proportionality

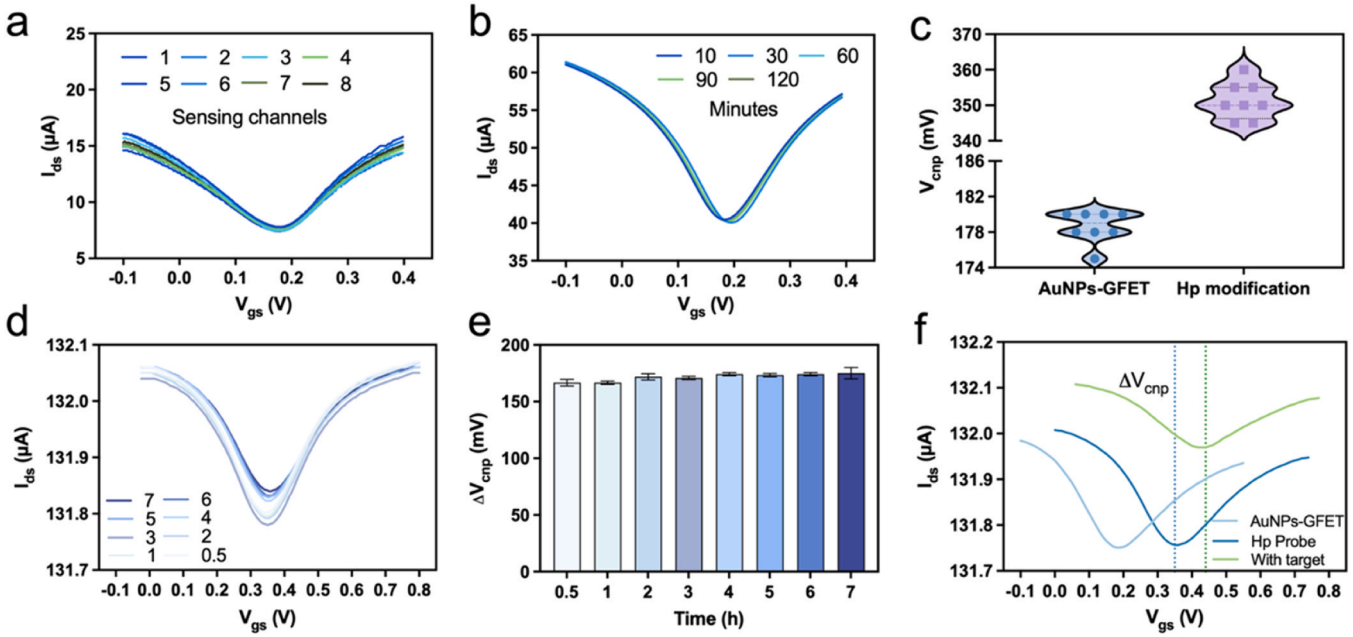

Fig. 3. The reliability of GFETs for the detection. (a) Reproducibility: transfer curves of 8 sensing channels measured at V_{ds} = 50 mV. (b) Stability: transfer curve of the GFET measured with respect to time. (c) V_{cnp} distribution of 8 GFETs measured at V_{ds} = 50 mV before and after the Hp modification. Transfer curves (d) and corresponding quantitative analysis (e) of GFETs after Hp modification during incubation. (f) Transfer curves of the AuNPs-GFET after each step of functionalization.

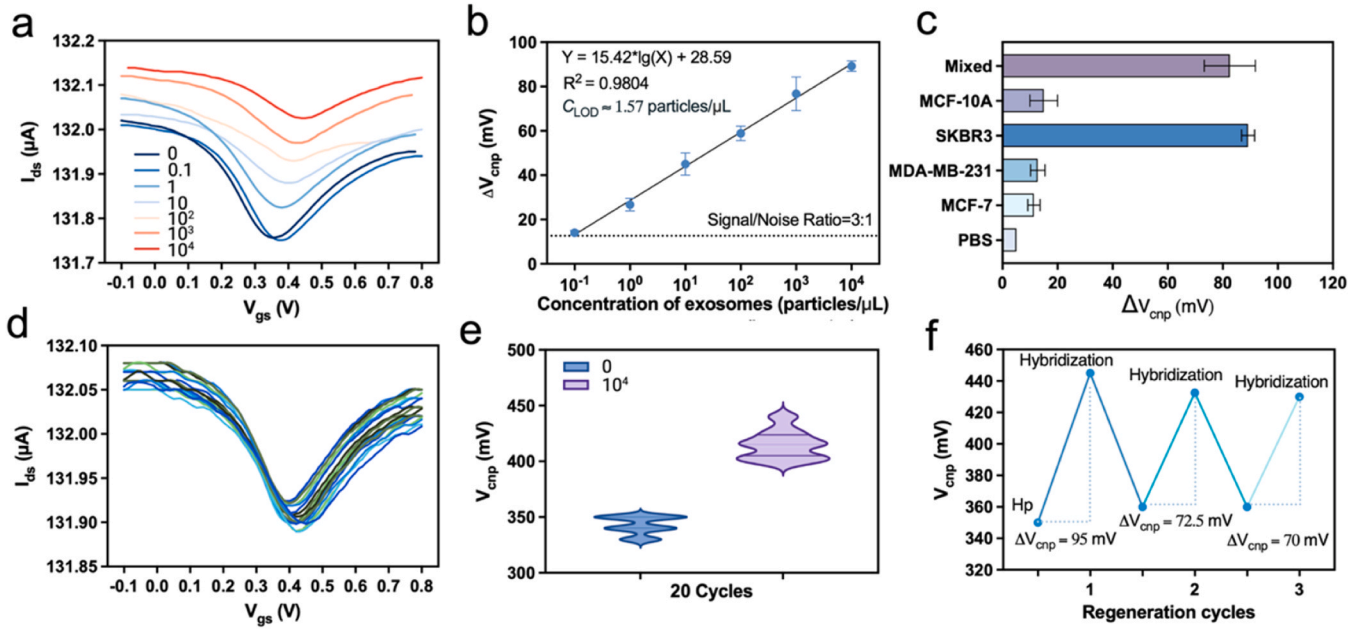

Fig. 4. The performance of the 3D DNA walker-powered GFET platform for exosomes detection. Sensitivity: Transfer curve (a) and corresponding calibration curves (b, n = 6) conducted with HER2-positive exosomes ranging from 0.1 particle/μL to 10^4 particles/μL at V_{ds} = 50 mV, S/N = 3. (c) Selectivity: ΔV_{cnp} response upon MCF-10A, PBS, MCF-7, MDA-MB-231, SKBR3 exosomes (HER2-positive exosomes) and mixture containing the above exosomes, V_{ds} = 50 mV. Error bars are obtained from three devices. (d) Reproducibility: Transfer curves recorded with 20 consecutive cycles and corresponding V_{cnp} distribution (e) conducted with 10^4 particles/μL of HER2-positive exosomes. (f) Reusability of the GFET using TCEP to detain the Hp probe conducted with 10^4 particles/μL of HER2-positive exosomes.

between the number of target exosomes binding events and the accumulation of negatively charged ssDNA-Hp complexes at the GFET interface. Linear regression analysis of the calibration curve yielded Y = 15.42*lg(X) + 28.59 (R^2 = 0.9804), indicating excellent linearity across five orders of magnitude. The LOD was calculated to be 1.57 particles/μL based on the blank signal plus 3 times the standard deviation (Fig. 4b). This ultrahigh sensitivity exceeds that of most reported exosome detection methods (Table S2), highlighting the advantages of integrating DNA walker-mediated signal amplification with FET conversion. Specifically, this design (i) provides molecular amplification, in which a single exosome-binding event generates multiple DNA reporter products; (ii) improves electrostatic coupling under ionic screening because the short ssDNA reporters hybridize close to the graphene surface, whereas intact exosomes (30–150 nm) place most charges farther from the sensing interface [34]; and (iii) allows the signal amplification step to be optimized independently of GFET readout conditions, thereby

improving measurement robustness and reproducibility. To further verify the signal transduction mechanism, the relationship between ssDNA concentration and GFET response was examined. The linear regression analysis exhibited a good linear correlation between ssDNA concentration and ΔV_{cnp} ($Y = 2.088*(X) + 8.264$, $R^2 = 0.9874$), which confirms that the released ssDNA serves as the direct mediator of the electrical response (Fig. S8). To evaluate the selectivity of the platform, exosomes derived from HER2-positive SKBR3 cells, HER2-negative breast cancer cell lines (MCF-7 and MDA-MB-231), a normal breast epithelial cell line (MCF-10 A), and mixed samples were tested under the optimized assay conditions (Fig. 4c). SKBR3 exosomes induced a pronounced V_{cnp} shift of 95 mV, whereas MCF-10 A, MCF-7, and MDA-MB-231 exosomes produced negligible shifts comparable to the PBS blank, indicating low nonspecific response. In mixed samples, SKBR3 exosomes spiked into two HER2-negative and normal exosomes retained 92% of the SKBR3 group signal, confirming high specificity under complex conditions. The transfer curves in Fig. S9 further demonstrated these results.

To evaluate the reproducibility and leakage current behavior of the device, 20 consecutive measurements were performed using HER2-positive exosomes, with PBS buffer as the blank. As shown in Fig. 4d, the V_{cnp} shifts remained tightly clustered across all cycles (RSD < 5%),

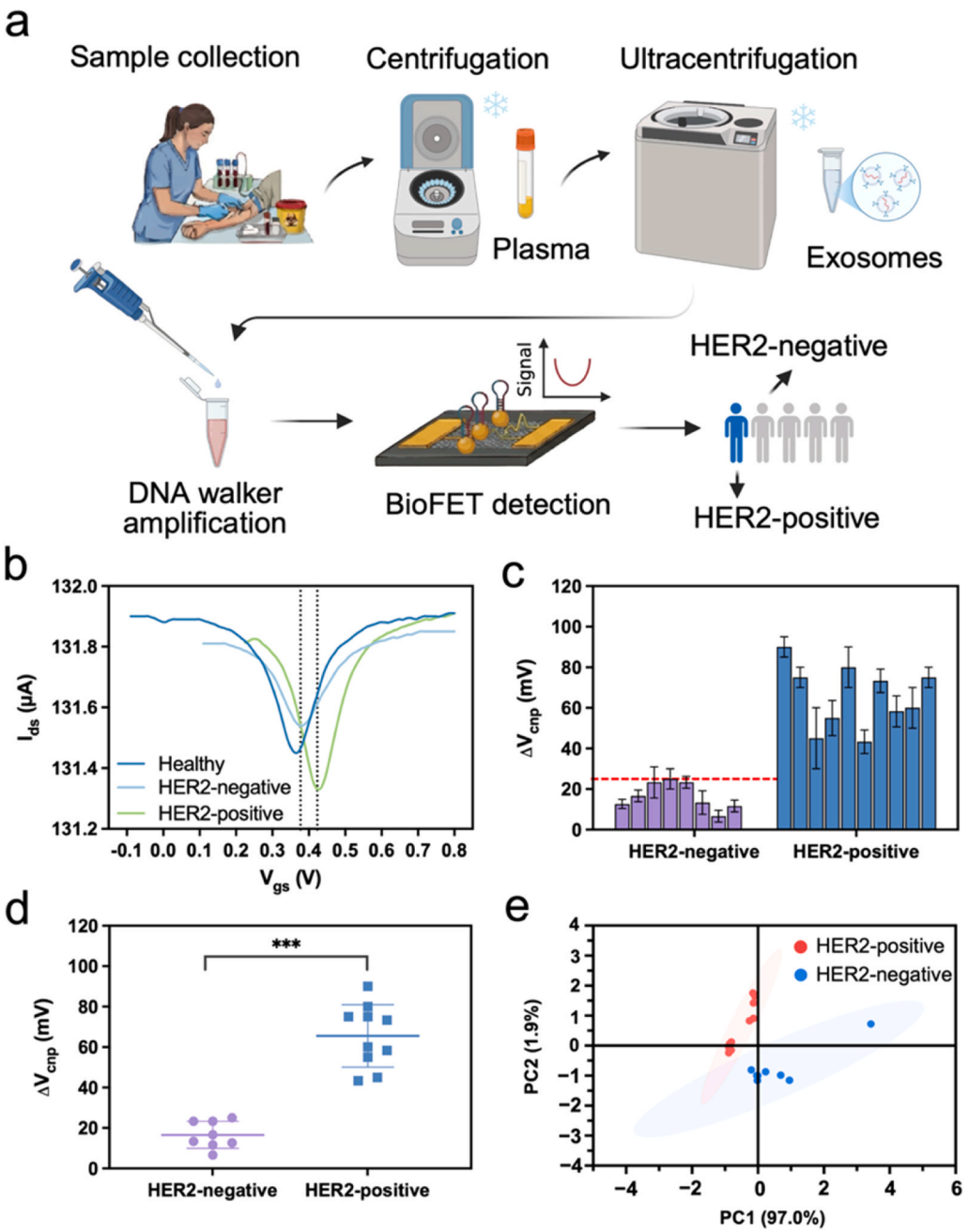

Fig. 5. Clinical sample analysis. (a) Schematic illustration of the 3D DNA walker-powered GFET platform for detecting HER2-positive exosomes using clinical plasma samples from breast cancer patients. (b) Transfer curves of the GFETs in the presence of exosomes extracted from healthy donors, HER2-positive, and HER2-negative patients. (c) Analysis of V_{cnp} shift collected from HER2-negative patients (n = 8) and HER2-positive patients (n = 10). (d) Significant expression difference of HER2-positive exosomes levels between HER2-positive and HER2-negative patients (***: $p < 0.001$). (e) PCA of transfer curves. The data were classified using 95% confidence ellipses. The differences in the data were analyzed by PC1 and PC2 (accounting for 97.0% and 1.9% of the variance, respectively), accounting for 98.9% of the total variance.

demonstrating excellent signal reproducibility. However, a gradual decrease in off-state current was observed in both exosomes and PBS samples, indicating baseline drift under continuous gate stress. Critically, this leakage current behavior was independent of the exosomes-induced signal and appeared identically in PBS blanks, confirming that the drift is intrinsic to the GFET device rather than assay failure (Fig. 4e). This phenomenon, consistent with previously reported behavior in FET devices, reflects charge trapping and dielectric polarization at the gate oxide interface under prolonged electrical stress [35]. Finally, device reusability was evaluated over three consecutive detection cycles with TCEP-mediated surface regeneration (Fig. 4f). Between cycles, TCEP treatment reduced disulfide bonds and released bound Hp-ssDNA complexes, which were then rinsed with deionized water and dried with nitrogen. Signal amplitude fully recovered in the first test but decreased to approximately 80% in the second and third cycles, likely due to the partial loss of Hp probes from incomplete dissociation of Hp-ssDNA complexes during TCEP treatment or minor surface fouling. Despite this decline, the retention of ~80% signal in cycles 2–3 demonstrates that the platform maintains good reusability and detection capability across multiple reuse cycles.

3.6. Clinical sample analysis

We further evaluated the performance of the DNA walker-powered GFET platform for detecting HER2-positive exosomes using clinical plasma samples from breast cancer patients (Fig. 5a). As shown in Fig. 5b, the V_{cnp} shift of HER2-positive breast cancer patients was significantly larger than that of HER2-negative breast cancer patients and healthy subjects, supporting the applicability of the platform in clinically relevant matrices. To assess the reliability of differentiating HER2-positive from HER2-negative cases, 18 plasma samples were randomly collected from the Third Affiliated Hospital of Sun Yat-sen University (Guangzhou, China), including 10 HER2-positive breast cancer patients ($n = 10$) and 8 HER2-negative breast cancer patients ($n = 8$). Analysis of individual patient data revealed that the ΔV_{cnp} responses in HER2-positive patients were markedly higher than those in HER2-negative patients ($p < 0.001$), consistent with clinical HER2 diagnostic results (Fig. 5c-d). Principal component analysis (PCA) further demonstrated group separation, with HER2-positive and HER2-negative samples forming distinct clusters along PC1 and PC2, indicating that the DNA walker-powered GFET platform can reliably distinguish HER2 status in clinical plasma samples (Fig. 5e).

The above results demonstrated the significant value of the proposed platform in clinical scenarios requiring accurate HER2 status determination. HER2 assessment is a routine and crucial component of breast cancer diagnosis, as it directly guides a patient's suitability for HER2-targeted therapy, such as trastuzumab [2,36]. Beyond distinguishing HER2-positive from HER2-negative patients, the DNA walker-driven GFET platform provides rapid, highly repeatable electrical signal readings, supports longitudinal monitoring, and enables continuous measurements to track therapy-associated changes in HER2-positive exosomal signals. In the post-treatment setting, the platform's ultrasensitive performance may also facilitate minimal residual disease surveillance and allow early detection of recurrence. Finally, the compact, label-free electrical transduction is well-suited to point-of-care or near-patient testing.

4. Conclusions

We established the first 3D DNA walker-powered GFET platform for ultrasensitive detection of HER2-positive breast cancer exosomes. In this system, AuNP-based DNA walkers are activated by target exosome recognition and catalytically generate abundant ssDNA reporters, which subsequently hybridize with hairpin probes immobilized on the GFET surface to convert molecular amplification into a strongly enhanced electrical response. The platform achieved rapid and quantitative detection within 1.5 h, with an ultralow limit of detection of 1.57 particles/μL. The assay exhibits high selectivity toward HER2-positive exosomes, robust analytical performance with excellent reproducibility (RSD < 5%), and practical reusability (~80% signal retention after regeneration). In addition, the platform has been successfully applied to test HER2 status in clinical samples, effectively distinguishing HER2-positive from HER2-negative breast cancer patients. Although the current workflow still involves multiple manual steps and the clinical dataset remains limited, this study establishes a generalizable framework that integrates programmable DNA nanomachines with GFET bioelectronics to enable sensitive, scalable, and electronics-ready exosome diagnostics. Future efforts will prioritize validation in larger, clinically diverse cohorts and system-level integration with on-chip microfluidics to deliver automated, sample-to-answer operation suitable for point-of-care deployment.

Supplementary Information

The Supporting Information is available free of charge at Document details the materials and methods section, additional figures and tables including experimental conditions optimization, quantitative analysis of substrate strands upload, DLS analysis for exosomes stability, EDS analysis of AuNPs-GFET, AFM analysis of pristine GFET, KPFM characterization of device before and after probe immobilization, GFET response to ssDNA, specificity curves of the system, table of oligo sequence, and comparison with other methods.

CRediT authorship contribution statement

Duo Wai-Chi Wong: Visualization, Validation. **Keyu Yao:** Visualization, Investigation. **Kunpeng Hu:** Supervision, Resources. **Mo Yang:** Supervision, Resources, Methodology. **Wen Yin:** Validation, Investigation, Data curation. **Xiao Shu:** Visualization, Methodology, Investigation, Data curation. **Haitian Chen:** Validation, Investigation. **Xijing Yan:** Validation, Investigation. **James Chung-Wai Cheung:** Writing – review & editing, Supervision, Resources. **Jingyu Shi:** Writing – review & editing, Supervision, Resources, Formal analysis, Conceptualization. **Quan Wang:** Writing – original draft, Visualization, Methodology, Investigation, Formal analysis, Data curation.

Declaration of Competing Interest

The authors declare that they have no known competing financial interests or personal relationships that could have appeared to influence the work reported in this paper.

Acknowledgment

This work was supported by Innovation and Technology Fund of Innovation and Technology Commission (Partnership Research Programme, PRP/003/24FX), and Start-up Fund for RAPs under the Strategic Hiring Scheme (1-BDV1) and additional funding (1-WZDC) from the Department of Biomedical Engineering of the Hong Kong Polytechnic University (PolyU, University Grant Council).

Appendix A. Supporting information

Supplementary data associated with this article can be found in the online version at doi:10.1016/j.snb.2026.139957.

Data availability

Data will be made available on request.

References

[1] H. Wang, Y. Zhang, H. Zhang, H. Cao, J. Mao, X. Chen, L. Wang, N. Zhang, P. Luo, J. Xue, Liquid biopsy for human cancer: cancer screening, monitoring, and treatment, MedComm 5 (6) (2024) e564, https://doi.org/10.1002/mco2.564.

[2] A.C. Wolff, M.E.H. Hammond, K.H. Allison, B.E. Harvey, P.B. Mangu, J.M. Bartlett, M. Bilous, I.O. Ellis, P. Fitzgibbons, W. Hanna, Human epidermal growth factor receptor 2 testing in breast cancer: American Society of Clinical Oncology/College of American Pathologists clinical practice guideline focused update, Arch. Pathol. Lab Med 142 (11) (2018) 1364–1382, https://doi.org/10.5858/arpa.2018-0902-SA.

[3] K.H.W. Ho, H. Lai, R. Zhang, H. Chen, W. Yin, X. Yan, S. Xiao, C.Y.K. Lam, Y. Gu, J. Yan, SERS-based droplet microfluidic platform for sensitive and high-throughput detection of cancer exosomes, ACS Sens 9 (2024) 4860–4869, https://doi.org/10.1021/acssensors.4c01357.

[4] L. Ma, H. Guo, Y. Zhao, Z. Liu, C. Wang, J. Bu, T. Sun, J. Wei, Liquid biopsy in cancer: current status, challenges and future prospects, Signal Transduct. Target Ther. 9 (1) (2024) 336, https://doi.org/10.1038/s41392-024-02021-w.

[5] L.E. Raez, K. Brice, K. Dumais, A. Lopez-Cohen, D. Wietecha, P.A. Izquierdo, E. S. Santos, H.W. Powery, Liquid biopsy versus tissue biopsy to determine front line therapy in metastatic non-small cell lung cancer (NSCLC), Clin. Lung Cancer 24 (2) (2023) 120–129, https://doi.org/10.1016/j.cllc.2022.11.007.

[6] H.L. Tran, W. Zheng, D.A. Issadore, H. Im, Y.-K. Cho, Y. Zhang, D. Liu, Y. Liu, B. Li, F. Liu, Extracellular vesicles for clinical diagnostics: from bulk measurements to single-vesicle analysis, ACS nano 19 (31) (2025) 28021–28109, https://doi.org/10.1021/acsnano.5c00706.

[7] T. Zhao, Y. Chen, W. Liu, X. Mo, X. Qin, Y. Yang, M. Fang, X. Li, W. Liu, F. Yang, Ultrasensitive profiling of plasma extracellular vesicles for breast cancer subtyping with a high-curvature antifouling nanoarray, Nano Lett. 25 (23) (2025) 9327–9336, https://doi.org/10.1021/acs.nanolett.5c01678.

[8] Y. Zhang, X. Qin, Z. Xu, W. Liu, H. Lu, Y. Yang, J. Yang, X. Li, Y. Zhang, F. Yang, Electric field-resistant bubble-enhanced wash-free profiling of extracellular vesicle surface markers, ACS nano 19 (8) (2025) 8093–8107, https://doi.org/10.1021/acsnano.4c16353.

[9] B. Wei, Y. Xiang, X. Qin, Y. Yang, H. Lu, H. Li, M. Fang, X. Li, F. Yang, EVs-on-a-bubble: self-aggregated click bubbles streamline isolation and amplified profiling of circulating extracellular vesicles, Adv. Funct. Mater. 34 (13) (2024) 2310823, https://doi.org/10.1002/adfm.202310823.

[10] Y. Wei, B. Wei, X. Mo, X. Xu, J. Huang, H. Lu, X. Qin, X. Li, F. Lin, F. Yang, Bubble multimer-enhanced fluorescence enables self-contained profiling of colorectal cancer extracellular vesicles, Nano Lett. 25 (46) (2025) 16411–16420, https://doi.org/10.1021/acs.nanolett.5c04275.

[11] X. Qin, Y. Xiang, L. Mao, Y. Yang, B. Wei, H. Lu, X. Li, Y. Zhang, F. Yang, Buoyant metal–organic framework corona-driven fast isolation and ultrasensitive profiling of circulating extracellular vesicles, ACS nano 18 (22) (2024) 14569–14582, https://doi.org/10.1021/acsnano.4c02339.

[12] D. Sung, J. Koo, A review of BioFET's basic principles and materials for biomedical applications, Biomed. Eng. Lett. 11 (2) (2021) 85–96, https://doi.org/10.1007/s13534-021-00187-8.

[13] Y. Zhu, Q. Wei, Q. Jin, G. Li, Q. Zhang, H. Xiao, T. Li, F. Wei, Y. Luo, Polyethylene glycol functionalized silicon nanowire field-effect transistor biosensor for glucose detection, Nanomaterials 13 (3) (2023) 604, https://doi.org/10.3390/nano13030604.

[14] W. Zhao, J. Hu, J. Liu, X. Li, S. Sun, X. Luan, Y. Zhao, S. Wei, M. Li, Q. Zhang, C. Huang, Si nanowire Bio-FET for electrical and label-free detection of cancer cell-derived exosomes, Micro Nanoeng. 8 (2022) 57, https://doi.org/10.1038/s41378-022-00387-x.

[15] D. Kwong Hong Tsang, T.J. Lieberthal, C. Watts, I.E. Dunlop, S. Ramadan, A.E. del Rio Hernandez, N. Klein, Chemically functionalised graphene FET biosensor for the label-free sensing of exosomes, Sci. Rep. 9 (1) (2019) 13946, https://doi.org/10.1038/s41598-019-50412-9.

[16] T. Yin, J. Song, X. Hao, Y. Wen, P. Yang, C. Gao, R. Cui, D. Li, Y. Hu, L. Xu, S. Ramadan, Engineering graphene field-effect transistor biosensors for disease biomarkers detection in liquid biopsy, ACS nano 20 (1) (2026) 163–207, https://doi.org/10.1021/acsnano.5c18891.

[17] Y. Wang, P. Li, Z. Liu, J. Kang, K. Liu, Y. Sun, C. Zhao, J. Tang, J. Cheng, Highly stretchable and reliable graphene-based strain sensor for plant health monitoring and deep learning-assisted crop recognition, Research 8 (2025) 0933, https://doi.org/10.34133/research.0933.

[18] Q. Wang, Z.-A. Zhao, K.-Y. Yao, Y.-L. Cheng, D.S.-H. Wong, D.W.-C. Wong, J.C.-W. Cheung, The versatility of biological field-effect transistor-based biosensors (BioFETs) in point-of-care diagnostics: applications and future directions for peritoneal dialysis monitoring, Biosensors 15 (3) (2025) 193, https://doi.org/10.3390/bios15030193.

[19] C.-H. Chu, I. Sarangadharan, A. Regmi, Y.-W. Chen, C.-P. Hsu, W.-H. Chang, G.-Y. Lee, J.-I. Chyi, C.-C. Chen, S.-C. Shiesh, Beyond the Debye length in high ionic strength solution: direct protein detection with field-effect transistors (FETs) in human serum, Sci. Rep. 7 (1) (2017) 5256, https://doi.org/10.1038/s41598-017-05426-6.

[20] J. Chen, Z. Luo, C. Sun, Z. Huang, C. Zhou, S. Yin, Y. Duan, Y. Li, Research progress of DNA walker and its recent applications in biosensor, TrAC Trends Anal. Chem. 120 (2019) 115626, https://doi.org/10.1016/j.trac.2019.115626.

[21] H. Linke, B. Höcker, K. Furuta, N.R. Forde, P.M.G. Curmi, Synthetic biology approaches to dissecting linear motor protein function: towards the design and synthesis of artificial autonomous protein walkers, Biophys. Rev. 12 (2020) 1041–1054, https://doi.org/10.1007/s12551-020-00717-1.

[22] L. Song, Y. Zhuge, X. Zuo, M. Li, F. Wang, DNA walkers for biosensing development, Adv. Sci. 9 (18) (2022) 2200327, https://doi.org/10.1002/advs.202200327.

[23] A.J. Thubagere, W. Li, R.F. Johnson, Z. Chen, S. Doroudi, Y.L. Lee, G. Izatt, S. Wittman, N. Srinivas, D. Woods, A cargo-sorting DNA robot, Science 357 (6356) (2017) eaan6558, https://doi.org/10.1126/science.aan6558.

[24] Y. Wang, C. Shen, C. Wu, Z. Zhan, R. Qu, Y. Xie, P. Chen, Self-assembled DNA machine and selective complexation recognition enable rapid homogeneous portable quantification of lung cancer CTCs, Research 7 (2024) 0352, https://doi.org/10.34133/research.0352.

[25] J. Wu, J. An, W. Li, Z. He, L. Lu, Sensitive electrochemical biosensor for exosome detection based on G-quadruplex track-guided DNA walker, Microchem. J. 212 (2025) 113538, https://doi.org/10.1016/j.microc.2025.113538.

[26] B. Mun, R. Kim, H. Jeong, B. Kang, J. Kim, H.Y. Son, J. Lim, H.W. Rho, E.-K. Lim, S. Haam, An immuno-magnetophoresis-based microfluidic chip to isolate and detect HER2-Positive cancer-derived exosomes via multiple separation, Biosens. Bioelectron. 239 (2023) 115592, https://doi.org/10.1016/j.bios.2023.115592.

[27] R. Kim, B. Mun, S. Lim, C. Park, J. Kim, J. Lim, H. Jeong, H.Y. Son, H.W. Rho, E. K. Lim, Colorimetric detection of HER2-overexpressing-cancer-derived exosomes in mouse urine using magnetic-polydiacetylene nanoparticles, Small 20 (13) (2024) 2307262, https://doi.org/10.1002/smll.202307262.

[28] L. Wang, Z.-J. Liu, H.-X. Cao, G.-X. Liang, Ultrasensitive colorimetric miRNA detection based on magnetic 3D DNA walker and unmodified AuNPs, Sens. Actuators B. 337 (2021) 129813, https://doi.org/10.1016/j.snb.2021.129813.

[29] D. Mazumdar, N. Nagraj, H.-K. Kim, X. Meng, A.K. Brown, Q. Sun, W. Li, Y. Lu, Activity, folding and Z-DNA formation of the 8-17 DNAzyme in the presence of monovalent ions, J. Am. Chem. Soc. 131 (15) (2009) 5506–5515, https://doi.org/10.1021/ja8082939.

[30] M. Gijs, G. Penner, G.B. Blackler, N.R. Impens, S. Baatout, A. Luxen, A.M. Aerts, Improved aptamers for the diagnosis and potential treatment of HER2-positive cancer, Pharmaceuticals 9 (2) (2016) 29, https://doi.org/10.3390/ph9020029.

[31] K.E. Katsuba, L.M. Zabegina, D.S. Plevako, A.A. Gurtovenko, A.V. Malek, Targeting HER2 with DNA aptamers for efficient anticancer drug delivery: a combined experimental and computational study, Bioconjugate Chem. 36 (2025) 1180–1196, https://doi.org/10.1021/acs.bioconjchem.5c00022.

[32] D. Li, W. Lai, D. Fan, Q. Fang, Protein biomarkers in breast cancer-derived extracellular vesicles for use in liquid biopsies, Am. J. Physiol. Cell Physiol. 321 (5) (2021) C779–C797, https://doi.org/10.1152/ajpcell.00048.202.

[33] F. Zhang, W. Shi, L. Guo, S. Liu, J. He, The Programmable Catalytic Core of 8-17 DNAzymes, Molecules 29 (11) (2024) 2420, https://doi.org/10.3390/molecules29112420.

[34] Y. Yu, Y.-T. Li, D. Jin, F. Yang, D. Wu, M.-M. Xiao, H. Zhang, Z.-Y. Zhang, G.-J. Zhang, Electrical and label-free quantification of exosomes with a reduced graphene oxide field effect transistor biosensor, Anal. Chem. 91 (16) (2019) 10679–10686, https://doi.org/10.1021/acs.analchem.9b01950.

[35] R. Ahmed, M. Sams, C. Simbrunner, M. Ullah, K. Rehman, G. Schwabegger, H. Sitter, T. Ostermann, Reproducibility and stability of C60 based organic field effect transistor, Synth. Met. 161 (2012) 2562–2565, https://doi.org/10.1016/j.synthmet.2011.08.008.

[36] J. Gorospe, M. Shapiro, V.R. Simhadri, Analyses of exosomal HER2 in breast cancer and the effect of respective exosome-immune complexes on trastuzumab-based immunotherapy, Int. J. Mol. Sci. 26 (21) (2025) 10331, https://doi.org/10.3390/ijms262110331.